Path Planning for Robot Based Radial Advanced Manufacturing Using Print Space Sampling

Nuwan Munasinghe and Gavin Paul

Centre for Autonomous Systems
University of Technology Sydney
{*Nuwan.Munasinghe, Gavin.Paul*}*@uts.edu.au*

***Abstract*— The world is embracing the fourth industrial revolution, Industry 4.0, which is enabling businesses to improve efficiency and optimise operations. The authors are part of a team that is researching and developing a large-scale industrial 3D printer to print smart, bespoke equipment called Gravity Separation Spirals (GSS). GSS are used in mining to separate minerals from the slurry. The printer under development employs two industrial robot arms mounted on vertical rails and the print direction is around a vertical rotating column in a radial direction. This paper presents a cost-based path planning method using print-space sampling to optimise distance error and manipulability during a printhead's radial path as it travels outwards from the central column. Manipulability, distance error and rotation error have been calculated for each sampled point and a weighted cost function has been used to determine the optimal path. Simulated results show that this method reduces the instances of print failure and improves the overall manipulability of the robot during printing.**

***Index Terms*— Industry 4.0, Advanced manufacturing, 3D printing, Industrial robots, Path planning**

I. Introduction

Additive manufacturing (AM), also known as 3D printing, is the process of manufacturing 3D objects from a computer model by depositing successive layers of material. This process can reduce both the lead time and material wastage, and enables a myriad of customisation possibilities. Also, this process enables the manufacturing of complex, bespoke, high-precision and intricate structures, which in turn provides design flexibility and improved customisation [1]. AM technology is evolving from a rapid prototyping tool into a viable alternative for end-product manufacturing [2]. Therefore, a large number of industries like construction, aviation and medicine are increasingly applying this technology [3]–[7].

The motivation for this project comes from the mining industry. Gravity Separation Spirals (GSS) are used around the world to separate minerals from slurry. The slurry is poured to the top of the GSS and it flows down the spiral. The carefully-engineered contour and slope of the GSS, naturally separates the slurry into certain desirable constituent minerals, which can then be collected at the bottom of the spiral. Fig. 1a shows a GSS manufacturing facility and Fig. 1b shows banks of spirals operating on-site. The properties of the slurry and the types of minerals being separated by a spiral dictates the most desirable profile of that spiral. Therefore, for each customer, the shape of the spiral would ideally be customised. However, such customisation would be highly uneconomical due to the time and labour involved with traditional mould-based manufacturing. Therefore, a research and development project is underway to design and build a 3D printer to print these GSS. Fig. 1c shows a one-third-of scale prototype printer that the engineering team has developed. Currently, the team is developing a full-scale printer Fig. 1d, which has two ABB robotic arms moving along vertical rails [8]. The central column of the printer is carefully rotated and the two robot arms manipulate a tool to extrude material on to this column and add layers that expand radially outwards. This paper addresses the problem of finding the optimal path the arm should take as it moves radially outwards during the printing process.

The dexterity of a robotic arm that enables it to move easily in any given direction is referred to as its manipulability [9]. When a robot arm has more dexterity it can perform additional actions, and such dexterity can enable added assembly or printing actions to occur, resulting in better utilisation of the robotic equipment. As well as developing a GSS 3D printer, our team is also researching and developing sensors that can be printed inline, or embedded inside the spiral. A smart GSS could enable remote monitoring of operation conditions, which is beneficial since the spirals operate in various remote parts of the world. Some of these novel sensors are 3D printable and can measure parameters like wear, strain and flow rate [10]–[13]. In order to print sensors inline, it is advantageous to maintain high manipulability throughout the print, since the sensors can have different complex shapes and be printed or assembled from different materials. Hence, the manipulability measure can be used to optimise specific 3D printing tasks in this research.

The manipulability measure has been used in other research as the basis to improve the effectiveness of robots. Since manipulability is an effective tool in robotic manipulators, [14] et al. showed how a dynamic manipulability ellipsoid for redundant manipulators could improve results. Nagatani et al. [15] developed a method to do path planning in a mobile manipulator by maintaining a threshold amount

*This research is supported by UTS, The Commonwealth of Australia's Department of Industry, Innovation and Science (Innovative Manufacturing CRC Ltd) and Downer, via its subsidiary Mineral Technologies.

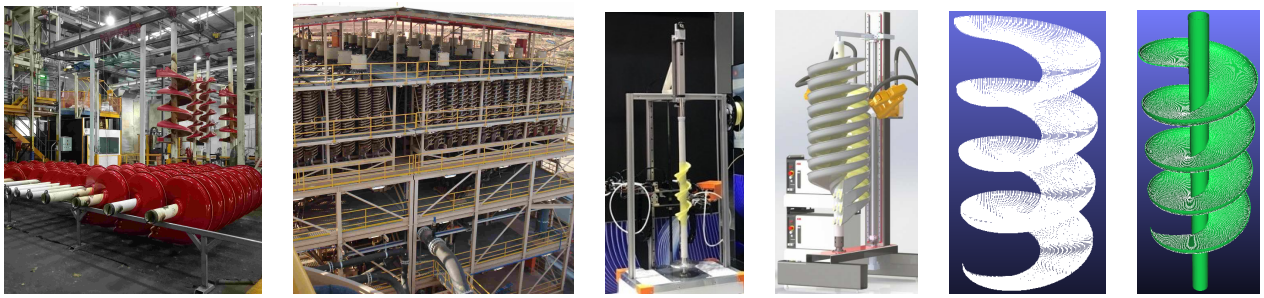

(a) (b) (c) (d) (e) (f)

Fig. 1: a) GSS manufacturing factory; b) Bank of GSS; c) One-third-of scale printer; d) Design of the full-scale; e) Way-points in the trajectories; f) Overlapped view of way-points and 3D model.

of manipulability. To determine high areas of manipulability researchers in the literature have employed and analysed a tool called manipulability area plots [15]. There are other applications where manipulability has been used to optimise the process. Amir et al. proposed a system which assists a human to teleoperate a remote arm [16]. They used a task-oriented velocity manipulability cost function. In another surgical robot application [17], a cost function incorporates the measures of distance from the joint limits and task-oriented manipulability during a suturing path to determine the optimal grasping pose of the needle. Manipulability-based optimal cutting path planning for legacy nuclear power plant equipment has been done by Tommaso et al. [18] where they used a multi-objective optimisation problem to maximise the robot's manipulability while minimising the travel distance. To generate a path from the start point to end-point, they used the rapidly-exploring random tree* algorithm.

In this research, cost-based path planning has been done to determine the radial path from the central column to the edge of the spiral rim. Cost-based path planning is common in many applications of robotics. An optimal path planning based on cost-based optimisation has been used for autonomous underwater vehicles [19]. They used the cost-based method to exploit the current data while avoiding obstacles. Their objective is to achieve greater speeds by getting advantage of river currents and minimising energy expenditure. Cost-based path planning has been used in humanoid navigation in uneven terrain [20], whereby both discrete planners and library-based planning was used to maximise efficiency. A cost-based graph search method was also used to calculate a path for the pose of the torso.

In this research, manipulability has been used as a performance measure of the robot arm in the printer space. A quality distribution map of the work-space has been used for humanoid robotic research to make various decisions, such as suitable grasp selection according to the current state [21]. This proposed method is also suitable for redundant manipulators as well while considering self-distance and joint limits. Probabilistic road maps (PRM) are a way of rapidly planning collision-free paths for robots. Manipulability-based bias sampling to generate PRM has been done and, in the configuration space, where manipulability is high, they took fewer samples and areas manipulability is low, they took more samples [22]. Path planning for redundant manipulators based on genetic algorithms and maximising manipulability has been proposed by Menasri et al [23]. This manipulability-based optimisation enables the system to move the robot in directions with less effort by exploiting the mechanical properties of the robot and avoiding the singularities.

We have developed a slicing algorithm to generate trajectories that can 3D print a GSS by moving a printhead in the shape of the spiral [24]. However, print failures could still occur, and finding a successful robot path required a non-systematic trial-and-error approach. Since there are multiple path options to progress towards the outer edge of the spiral, this research proposes a way to determine the optimal path to move the printhead radially outwards by considering a combined cost function to achieve a successful print and hence improve the overall manipulability.

This paper is organised as follows: Section II explains the problem in detail and then the proposed methodology; Section III presents experimental results and the discussion of the results, and finally, Section IV presents the conclusions.

II. Methodology

A. Problem and Simulation Environment

To print a GSS, a 3D model of the GSS is sliced into trajectories for the tooltip to follow. This algorithm has been developed [24]. Fig. 1e shows way-points in the generated trajectories from this algorithm and Fig.1f shows an overlapped view of the way-points and the 3D model of a GSS.

To simulate the printing process, a simulation environment has been developed in Matlab according to the actual dimension of the printer and robots (ABB IRB 120) and the robot is modeled using Denavit–Hartenberg (DH) parameters. The robot simulation has been done using the robotics toolbox developed by Peter Corke [25]. Fig. 2 shows the simulation environment in Matlab and the printing of the first trajectory.

During the printing process, the robot arm affixed with a printhead, starts by depositing the first layer of melted material on the rotating column. It then progressively adds

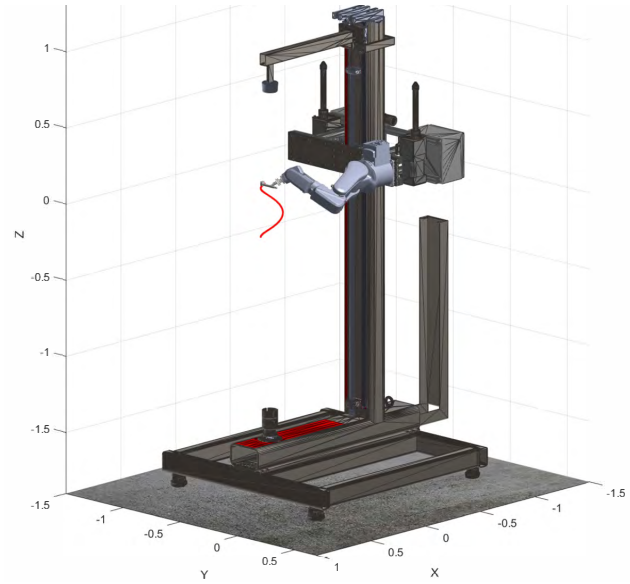

Fig. 2: Simulated printing the start of a single trajectory.

layer-upon-layer and expands the print radially outwards. Each layer has multiple trajectories and printing starts from the bottom and ends at the top. While printing a single layer, the robot arm gradually moves along a vertical rail from bottom to top in a vertical line and the central column rotates to achieve the helical shape. Fig. 3 shows a top-down view of the printer and the dashed lines shows these concentric vertical layers or cylinders. The problem that this paper addresses is discovering the path that should be taken when moving outwards from the central column. Since the location of the robot arm in the print space changes in order to cover a large print volume with a small robot arm, then the potential dexterity of the robot arm is also constantly changing. This ultimately affects the quality of the print and can cause major failures in the print. Fig. 3 shows a few example paths printhead can move in each layer. Theoretically, there are a massive number of possible paths that can be generated, some of which are undesirable or even infeasible, and this paper addresses the problem of finding the optimal path.

B. Proposed Solution

1) Manipulability: The ability of an industrial robotic arm to move easily in any arbitrary direction is called its manipulability [9]. Yoshikawa's manipulability measure describes an arm's distance to a singular configuration [26]. This approach is based on an analyses of the velocity ellipsoid that is spanned by the singular vectors of the Jacobian [26]. The Jacobian matrix shows the relationship between joint rates, $\dot{q}$ and the end-effector cartesian velocity, v as shown in Eq. (1), where q is the joint angles [9]. The manipulability can be calculated using the Jacobian matrix

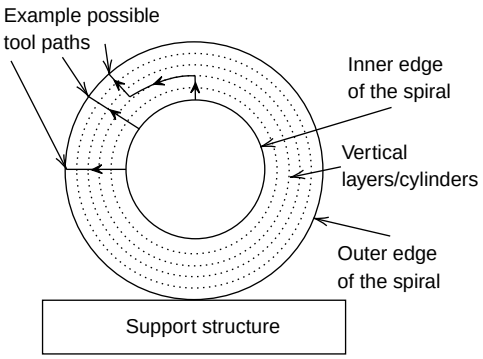

Fig. 3: Several examples of printhead movements paths.

as in Eq. (2).

$$v = J(q)\dot{q} \tag{1}$$

$$m = \sqrt{det\,(JJ^T)} \tag{2}$$

2) Proposed Cost Function: The aim of this research is to determine the optimal path to move the printhead from the closest cylinder near the central column, $i = 1$ to the last cylinder, $i = n$ where n is the total number of cylinders. Path planning depends on a cost function, which is a weighted combination of three cost values, inverse manipulability, $C_m(p)$ euclidean distance error, $C_d(p)$ and roll-pitch-yaw rotation error, $C_r(p)$ where p is a given sample location and p_c is the true location that printhead ends up in, when the system attempts to move it to p. p can be represented as a coordinate, (i, k) where i is the cylinder number and k is the k^{th} location in that cylinder. The weights of the manipulability, w_m distance error, w_d and rotation error, w_r are used in the combined cost function, Eq. (6).

$$C_m(p) = 1 - m(p) \tag{3}$$

$$C_d(p) = d(p_c, p) \tag{4}$$

$$C_r(p) = d_{roll}(p_c, p) + d_{pitch}(p_c, p) + d_{yaw}(p_c, p) \tag{5}$$

$$C(p) \;=\; w_m \cdot C_m(p) + w_d \cdot C_d(p) + w_r \cdot C_r(p) \tag{6}$$

Since the manipulability is a value between 0 and 1 (where a higher value is better), and it has been converted to a cost as shown in Eq. (3). The function $d(p_c, p)$ in Eq. (4) calculates the euclidean distance between p and p_c. Functions $d_{roll}(p_c, p)$, $d_{pitch}(p_c, p)$ and $d_{yaw}(p_c, p)$ calculates the absolute values of roll, pitch and yaw angle difference respectively between the p and p_c. Improving the distance error and rotation error will improve the accuracy of the original shape of the spiral. While improving the manipulability will help the manipulator to avoid singularities during the printing and result in an improved dexterity that can help to print sensors inline in future research. The weight values could be tuned to bias the cost function towards certain print objective, such as accuracy vs improved manipulability. A sensitivity analysis of the weights for the path is conducted in Section III.

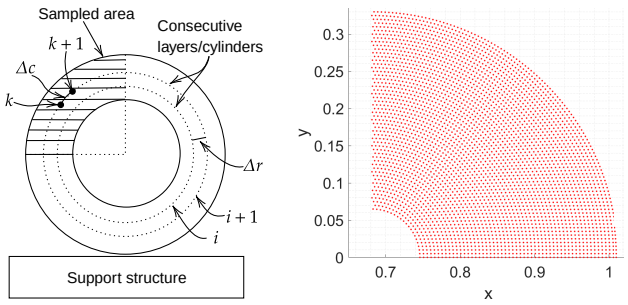

(a) (b)

Fig. 4: a) Sampled area. b) Generated sampling points.

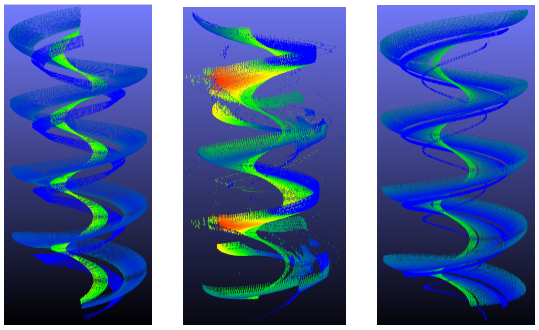

(a) (b) (c)

Fig. 5: Failed prints that did not use path planning.

3) Sampling of Print Space: Prior to planning the path, it is necessary to sample the print space to calculate different cost values as explained in the previous section at each sample location. An example of sampling has been done in the area shown in Fig. 4a where the robot arm can move easily without getting caught in poses which robot arm cannot reach. The granularity and number of samples depends on the user requirements. Fig. 4b shows these generated sample locations and Fig. 4a shows the user-defined parameters used to generate these sample locations: the distance between consecutive cylinders, Δr and distance between two consecutive sample locations in a single cylinder, Δc. The orientation of the printhead is set to be a constant value throughout all locations since in this case it is assumed that the printhead should be extruding material to the direction of the column. After generating these locations, the robot arm is moved to each sample location using an inverse kinematic solver, and various cost values mentioned in the previous section are calculated.

4) Path Planning: After calculating the cost values for each sample point, a path must be determined to navigate from one cylinder to another. For each cylinder, i, the minimum cost sample point, $p_{min,i}$ is selected as Eq. (7),

$$p_{min,i} = \underset{k}{\operatorname{argmin}} \; C(i,k) \tag{7}$$

$$P = [p_{min,1}, p_{min,2}, \ldots, p_{min,n}] \tag{8}$$

and the sequence of these points from $p_{min,1}$ to $p_{min,n}$ represents the optimal path as shown in Eq. (8). This path is followed during the full spiral printing

III. Experiment Results and Discussion

This section shows the results of the printing experiments conducted in the simulation environment. The resulting simulated prints are exported as a point cloud, where each point has a manipulability value, so that the results can be visualised easily. The first section shows the print results without path optimisation and failed prints, which motivated this research. Then the next sections visualise the cost values in the sampled space and results of the successful print. For all the experiments, the sampling was done using the parameter values of $\Delta r = 5mm$ and $\Delta c = 5mm$.

A. Results Without Optimal Path Planning

This section shows several failed prints and the indicative modes of failure when the optimal path planning method is not used. The colours in the print are related to the manipulability, where blue shades represent problematic values that are close to zero, the next increment is green, yellow and finally red shades as the values increase away from zero. Since higher values of manipulability are better, green, yellow then red indicate values that change from good to best. Fig. 5 shows the simulated printed results as point clouds. There are major print failures like 5b, or just a few trajectory failures like in 5c. The figures of the prints demonstrate a wider trend relating the level of failure with low levels of manipulability experienced by the robot arm. By using trial and error, it is conceivable that a printing path may be discovered but that is a time-consuming and non-systematic approach. Avoiding the wasteful print failures, through a systematic planning approach is the motivation behind this research paper.

B. Cost Values and Path Planning Results

Fig. 6 shows mesh plots of various cost values. The manipulability measure is converted to a cost as per Eq. (3). The weights for the combined cost function in Eq. (6) are selected as $w_m = w_d = 1$ and $w_r = 0.01$. Fig. 4b shows how the sampled locations are in an arc. To generate mesh plots, points in a 400-by-400 square grid were created and unknown values were interpolated using scattered interpolation method. Fig. 6e shows a contour plot of the same mesh plot of 6d with the generated path. Weights were chosen after conducting a path deviation analysis, while keeping the other two weights constant (value 1), and changing the selected weight from 0 to 1 as in Fig. 7. Weights were chosen to minimise three outcomes: path deviation, path length, and back-and-forth rotations, which thus reduce print times. Low weights were chosen for the rotation error because, from the sensitivity analysis, higher weights caused a higher path deviation. Similarly, the weighting factor for manipulability was set to be high, since it will reduce the path deviation. An unexpected result in Fig. 7 is how as the distance weight changes the rotation angle difference seems

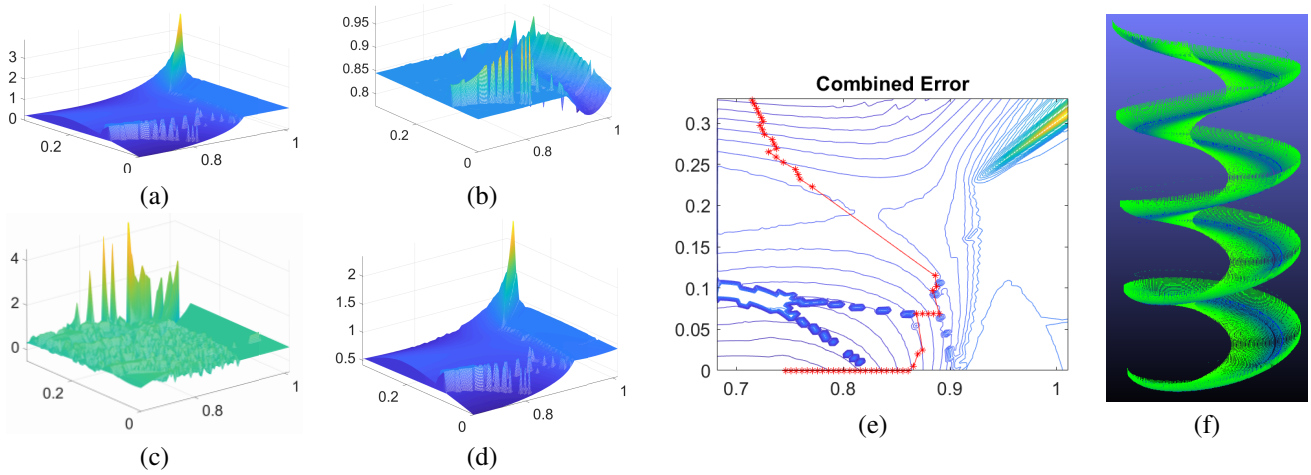

Fig. 6: Mesh plots: a) Inverse manipulability; b) Distance error; c) Rotation error; d) Combined error; e) Combined error contour plot with the generated path; (f) Successful print with the generated path.

low and surprisingly consistent. Further analysis showed this was since the peak values in Fig. 6a and Fig. 6b are at approximately the same location. Therefore, a change in the distance error value does not cause a significant path deviation as it was already avoided through consideration of the manipulability cost value.

It should be noted that the cost values and path change behaviours are unique to the kinematic model of the robot and the print dimension. Hence, different configurations will produce different results. However, the same methodology can be applied to any spiral print job or industrial robot model provided manipulability measures can be computed.

Fig. 6f shows a successful print where the path is generated using the presented optimal print path planing method. When this is compared with the failed prints in Fig. 5, it can be seen that there are no off-print trajectories and overall, the spiral is completely green. This means the manipulability values are higher, and not close to zero (i.e. awkward poses) as in the failed prints shown in Fig. 5.

IV. Conclusion

This paper has presented a path planning method for use in radial 3D printing. The method computes optimal movements of a printhead affixed to a small-workspace industrial robot mounted on a vertical rail. Path planning was done by sampling the print space and considering cost functions with weightings that effectively maximise the manipulability, whilst reducing the positional and rotation errors in overall printing. This has been shown to improve the accuracy and success of the printer. This path planning method thus solves the problem of failed prints by providing a systematic way of determining the path that can replace the original trial-and-error approach. Additionally, improved manipulability during the print helps with future research that looks to more effectively utilise the robot to enable inline sensor printing.

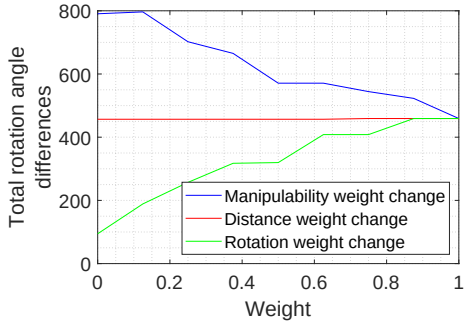

Fig. 7: Path deviation with weight change.

Acknowledgment

This research is supported by UTS, The Commonwealth of Australia's Department of Industry, Innovation and Science (Innovative Manufacturing CRC Ltd) and Downer, via its subsidiary Mineral Technologies. Thank you to Rapido, in particular, Hervé Harvard and Michael Behrens for establishing this overall research activity and leading the overall R&D engineering project. And to Jordan Henry, from UTS Rapido for creating the simulation environment of the printer. We also thank UTS:RI/CAS for providing required resources to carry out this research.

References

[1] CSRIO, "Advanced manufacturing : A Roadmap for unlocking future growth opporunities for Australia," Tech. Rep. November, 2016, pp. 4–7.

[2] K. V. Wong and A. Hernandez, "A Review of Additive Manufacturing," *ISRN Mechanical Engineering*, vol. 2012, no. 208760, p. 10, 2012.

[3] E. P. Flynn, "Low-cost approaches to UAV design using advanced manufacturing techniques," in *IEEE Conf. ISEC*, Mar. 2013, pp. 1–4.

[4] Y. Tadjdeh, "3D Printing Promises to Revolutionize Defense, Aerospace Industries," English, *National Defense*, vol. 98, no. 724, pp. 20–23, Mar. 2014.

[5] P. Shakor, S. Nejadi, G. Paul, and S. Malek, "Review of Emerging Additive Manufacturing Technologies in 3D Printing of Cementitious Materials in the Construction Industry," *Frontiers in Built Environment*, vol. 4, no. January, 2019.

[6] G. Z. Cheng, E. Folch, A. Wilson, R. Brik, N. Garcia, R. S. J. Estepar, J. O. Onieva, S. Gangadharan, and A. Majid, "3D Printing and Personalized Airway Stents," *Pulmonary Therapy*, vol. 3, no. 1, pp. 59–66, 2017.

[7] D. D. Camacho, P. Clayton, W. O'Brien, R. Ferron, M. Juenger, S. Salamone, and C. Seepersad, "Applications of Additive Manufacturing in the Construction Industry," in *ISARC*, vol. 34, Vilnius, 2017, pp. 1–8.

[8] E. Australia, *Milestone for mining manufacture with 3D printing*. [Online]. Available: `https://portal.engineersaustralia.org.au/news/milestone-mining-manufacture-3d-printing`.

[9] P. Corke, *Robotics Vision and Control*, 2 Edition, 1-2. Springer, 2015, vol. 75, pp. 197–200.

[10] M. I. N. P. Munasinghe, L. Miles, and G. Paul, "Direct-Write Fabrication of Wear Profiling IoT Sensor for 3D Printed Industrial Equipment," in *ISARC*, 2019, pp. 862–869.

[11] N. Munasinghe, M. Woods, L. Miles, and G. Paul, "3-D Printed Strain Sensor for Structural Health Monitoring," in *Int. Conf. CIS-RAM*, Bangkok: IEEE, 2019.

[12] N. Munasinghe and G. Paul, "Advanced Manufacturing of Spirals for Mineral Separation with Integrated Smart Sensing," in *IEEE UNITE*, 2019. [Online]. Available: `http://hdl.handle.net/10453/135218`.

[13] ——, "Ultrasonic-Based Sensor Fusion Approach to Measure Flow Rate in Partially Filled Pipes," *IEEE Sensors Journal*, vol. 20, no. 11, pp. 6083–6090, 2020.

[14] P. Chiacchio, "A new dynamic manipulability ellipsoid for redundant manipulators," *Robotica*, vol. 18, no. 4, pp. 381–387, 2000.

[15] K. Nagatani, T. Hirayama, A. Gofuku, and Y. Tanaka, "Motion planning for mobile manipulator with keeping manipulability," in *IEEE Int. Conf. on IROS*, vol. 2, 2002, pp. 1663–1668.

[16] E. A. M. Ghalamzan, F. Abi-Farraj, P. R. Giordano, and R. Stolkin, "Human-in-the-loop optimisation: Mixed initiative grasping for optimally facilitating post-grasp manipulative actions," in *Int. Conf. on IROS*, IEEE, 2017, pp. 3386–3393.

[17] M. Selvaggio, A. M. G. E, R. Moccia, F. Ficuciello, and B. Siciliano, "Haptic-guided shared control for needle grasping optimization in minimally invasive robotic surgery," in *Int. Conf. on IROS*, 2019, pp. 3617–3623.

[18] T. Pardi, V. Ortenzi, C. Fairbairn, T. Pipe, A. M. G. Esfahani, and R. Stolkin, "Planning Maximum-Manipulability Cutting Paths," *IEEE Robotics and Automation Letters*, vol. 5, no. 2, pp. 1999–2006, 2020.

[19] D. Kruger, R. Stolkin, A. Blum, and J. Briganti, "Optimal AUV path planning for extended missions in complex, fast-flowing estuarine environments," in *IEEE ICRA*, IEEE, 2007, pp. 4265–4270.

[20] Y.-C. Lin and D. Berenson, "Humanoid Navigation Planning in Large Unstructured Environments Using Traversability - Based Segmentation," in *Int. Conf. on IROS*, IEEE, 2018, pp. 7375–7382.

[21] N. Vahrenkamp, T. Asfour, G. Metta, G. Sandini, and R. Dillmann, "Manipulability analysis," in *RAS Int. Conf. on Humanoid Robots*, IEEE, 2012, pp. 568–573.

[22] P. Leven and S. Hutchinson, "Using manipulability to bias sampling during the construction of probabilistic roadmaps," in *ICRA*, vol. 2, IEEE, 2002, pp. 2134–2140.

[23] R. Menasri, A. Nakib, H. Oulhadj, B. Daachi, P. Siarry, and G. Hains, "Path planning for redundant manipulators using metaheuristic for bilevel optimization and maximum of manipulability," *IEEE Int. Conf. on ROBIO*, no. Dec. Pp. 145–150, 2013.

[24] N. Munasinghe and G. Paul, "Radial Slicing for Helical-Shaped Advanced Manufacturing Applications," *International Journal of Advanced Manufacturing Technology*, 2020.

[25] P. Corke, *Guestbook: Robotics Toolbox*. [Online]. Available: `http://www.petercorke.com/RTB/`.

[26] T. Yoshikawa, "Manipulability of Robotic Mechanisms," *International Journal of Robotics Research*, vol. 4, no. 2, pp. 3–9, 1985.